Applied Catalysis A: General 355 (2009) 132–138

Contents lists available at ScienceDirect

Applied Catalysis A: General

journal homepage: www.elsevier.com/locate/apcata

Characterization of nitric acid functionalized carbon black and its evaluation as electrocatalyst support for direct methanol fuel cell applications

Marcelo Carmo [a,b,*], Marcelo Linardi [b], João Guilherme Rocha Poco [a]

[a] Instituto de Pesquisas Tecnológicas do Estado de São Paulo, Av. Prof. Almeida Prado 532, Cid. Universitária, 05508-901 São Paulo, Brazil
[b] Instituto de Pesquisas Energéticas e Nucleares – IPEN/CNEN, Av. Prof. Lineu Prestes 2242, Cid. Universitária, 05508-000 São Paulo, Brazil

ARTICLE INFO

Article history:
Received 17 March 2008
Received in revised form 4 December 2008
Accepted 5 December 2008
Available online 11 December 2008

Keywords:
Carbon functionalization
HNO_3
Electrocatalysis
Fuel cell
PEMFC
DMFC

ABSTRACT

This study presents results on PtRu electrocatalysts supported on both as received and functionalized carbon black. The electrochemical properties of both home-made and commercial PtRu electrocatalysts were compared to PtRu supported on functionalized carbon black. The PtRu nanoparticles were synthesized by the impregnation method and subsequent alcohol reduction. Transmission electron microscopy experiments revealed that the PtRu electrocatalysts supported on functionalized carbon black are more homogeneously distributed than all other studied materials. Cyclic voltammetric electrocatalyst curves experiments showed higher activity for the PtRu supported on functionalized carbon black. This enhanced performance is related to the better nanoparticle distribution on functionalized carbon black. The better performance can also be inferred by the better nanoparticles utilization. The nanoparticles are now located outside from the pore structure of the carbon black. Hence, the nanoparticles are more exposed and available to the reactants, enhancing the catalyst performance and avoiding the waste of noble catalysts.

1. Introduction

Hydrogen is currently the most efficient and commonly used fuel for polymer electrolyte membrane fuel cell (PEMFC). However the cost of its production and the problems associated with its storage and distribution make the application of this fuel a challenge [1,2]. Several studies investigate the utilization of methanol as a fuel to operate the PEMFC [3–6]. In this case the cell is called as direct methanol fuel cell (DMFC). However, there are still drawbacks regarding the use of such a fuel. The electrochemical oxidation reaction of methanol is a less efficient process compared to the hydrogen oxidation. Poisoning intermediates are formed due to incomplete methanol oxidation, mainly carbon monoxide (CO). In order to overcome the CO poisoning, an alternative to favor the CO oxidation is the use of a second metal, e.g. ruthenium (Ru) [7]. The added Ru is able to form oxygenated species, facilitating the oxidation of the CO_{ads} to carbon dioxide (CO_2) at lower potentials than platinum. This phenomenon is called bifunctional mechanism and was first considered by Watanabe and Motoo [8]. Moreover, an electronic effect, which weakens the CO_{ads} bond on the surface and results in a higher power density for DMFC application was proposed [9]. Carbon black is frequently used as the catalyst support because of its relative high stability in both acid and basic media, good electronic conductivity and high specific surface area. The support material has a strong influence on the properties of the catalysts, such as metal particle size, electrochemical active area and size distribution. Furthermore, degree of alloying, stability, mass transport and electronic conductivity of the catalytic layer are also affected by the chosen support material. Hence, the optimization of carbon supports plays an important role for the future PEMFC technology. The support should be well selected, with a suitable specific surface area, porosity, morphology, surface functional groups and electronic conductivity. Corrosion resistance is also a crucial parameter to be considered, while developing an active commercial catalyst. Most of these parameters are affected by the process used to prepare the carbon black. Carbon black still reveals inadequacies for this purpose [10,11]. Consequently, the carbon support can be modified at the micro(nano)scopic level. One would be the chemical modification of the carbon black surface used to anchor the nanoparticles of the electrocatalysts. Chemical reactions could be applied to encapsulate, protect and change the hydrophobic/hydrophilic character of the materials. By this means, the reactivity can be changed, catalytic properties modified as well as, composites created and polarities changed (zeta potential) [12–17].

* Corresponding author at: Instituto de Pesquisas Tecnológicas do Estado de São Paulo, Av. Prof. Almeida Prado 532, Cid. Universitária, 05508-901 São Paulo, Brazil.
E-mail address: marcelocarmo1@gmail.com (M. Carmo).

0926-860X/$ – see front matter © 2008 Elsevier B.V. All rights reserved.
doi:10.1016/j.apcata.2008.12.010

In this study, functionalization of the carbon black surface by nitric acid treatment was carried out; introducing oxygenated functional groups, modifying its properties and hindering both agglomeration and/or loss of active surface.

2. Experimental

A commercial carbon black Vulcan XC72R (Cabot) was used as a support. This carbon was functionalized with concentrated nitric acid at 80 °C, refluxed for 24 h (sample labeled XC72R-HNO_3). The functionalized carbon was filtered, washed until water reached pH neutral and dried at 110 °C overnight. The functionalized carbon was labeled C-HNO_3.

Carbon-supported electrocatalysts were prepared through impregnation method and subsequent alcohol reduction [18–20]. A mixture of the desirable metallic ions solution was used as precursor, where the ions were reduced to their metal forms, using ethylene glycol (Merck) as solvent and reducing agent in the presence of the carbon support. PtRu/C (20 wt.%, Pt:Ru atomic ratio of 1:1) was prepared using this procedure. $H_2PtCl_6{\cdot}6H_2O$ (Aldrich) and $RuCl_3{\cdot}2H_2O$ (Aldrich) were used as metal sources. High surface area carbon black Vulcan XC-72R as delivered and functionalized carbon black C-HNO_3 were used as supports. In this procedure the salts were first added to the carbon support, followed by an ethylene glycol solution (75:25—ethylene glycol:water). The system was ultrasonically treated for 15 min. It was then refluxed and heated at 160 °C for 1 h. The resulting powder was filtered, washed with distillated water and dried in air at 110 °C overnight. PtRu/C (20 wt.%, Pt:Ru atomic ratio of 1:1) commercial electrocatalysts from Etek® Basf Fuel Cell Inc. was used for comparative purposes.

The chemical analysis of the surface functionalities was carried out following the Boehm method [21], which uses aqueous solutions of bases of different strengths to determine the acidic groups: carboxyls, lactones and phenols. For this purpose, different batches of 0.25 g of sample was in contact, at 298 K for 60 h, with 25 cm^3 of solutions of $NaHCO_3$ (0.1 M), Na_2CO_3 (0.05 M) and NaOH (0.1 M), respectively. Then the aqueous solutions were titrated with standard HCl. According to the method, $NaHCO_3$ neutralizes the carboxyl groups, lactones are determined by the difference between the groups neutralized by Na_2CO_3 and $NaHCO_3$ and the difference between the groups neutralized by NaOH and Na_2CO_3 is phenols. Moreover, the basic groups are analyzed in a similar way by neutralization with HCl solutions and further titration with NaOH.

A NOVA 300 Brunauer–Emmet–Teller (BET) analyzer was used to determine the specific surface area of the carbons. Prior to measurement, the carbon samples were purged with pure nitrogen gas overnight at a temperature of 150 °C to remove any contaminants and moisture that may have been present in the carbon support.

A laser scattering (LS) LS230 small volume module plus–coulter was used to estimate the average particle size of the carbons in an aqueous colloidal system. Before measuring, 5 mg of the sample was dispersed in water and sonicated for at least 48 h.

A thermal analysis system Star SDTA851^e module from Mettler/Toledo with Stare version SW 8.01 software was used for thermal gravimetric analysis at a heating rate of 10 °C min^{-1} from 25 to 1000 °C, in nitrogen flow at 50 mL min^{-1}.

Electrokinetic potentials (zeta potentials) for the carbon particles were determined by using a zeta probe zeta potential analyser–colloidal dynamics, 250 mg of sample was dispersed in 250 mL of 0.01 mol L^{-1} KCl solution, sonicated and magnetically stirred for at least 48 h before the measurements were carried out. To generate the zeta potential vs. pH curves and from them the isoelectric point or zero charge potential (E_{zc}), the pH of the slurry was adjusted using HCl and NaOH solutions, followed by mechanical stirring (usually 24 h).

The Pt:Ru atomic ratios of the electrocatalysts were obtained by using a Philips XL30 scanning electron microscope coupled to an EDAX DX-4 microanalyzer with a 20 keV electron beam.

The X-ray diffraction (XRD) analyses were performed using a STOE STADI-P diffractometer with germanium monochromized Cu Kα radiation and position-sensitive detector with 40 apertures in transmission mode. The X-ray diffractograms were obtained with a scan rate of 1° min^{-1} and an incident wavelength of 1.5406 Å (Cu Kα). The average crystallite size was estimated with the XRD data and the Scherer equation [22].

The transmission electron microscopy (TEM) characterization was done using a JEOL JEM-1200EX microscope and the average particle size was calculated using the Image Tool Software Lince with one TEM micrograph for each catalyst and counting 300 particles/picture.

Electrochemical studies of the electrocatalysts were carried out using the thin porous coating technique [23,24]. An amount of 10 mg of the electrocatalysts was added to 10 g of water. The mixture was submitted to an ultrasound bath for 5 min, where two drops of a 6% PTFE (polytetrafluorethylene) water suspension were added. Again, the mixture was submitted to an ultrasound bath for 5 min, filtered and transferred to the working electrode support cavity (0.30 mm deep and area of 0.36 cm^2). The quantity of the electrocatalysts in the working electrode was determined with a precision of 0.0001 g. In the cyclic voltammetry (CV) experiments, the current values (I) were expressed in Ampere and were normalized per gram of platinum ($Ag_{metal}{}^{1-}$). The reference electrode was an RHE (reversible hydrogen electrode) and the counter electrode was a platinized Pt net with 4 cm^2. Electrochemical measurements were taken using a Microquimica (model MQPG01, Brazil) potentiostat/galvanostat coupled to a computer and using the Microquimica Software. Cyclic voltammetry was performed in a 0.5 mol L^{-1} H_2SO_4 solution saturated with N_2.

The evaluation of the 1.0 mol L^{-1} methanol solution oxidation was performed at 25 °C in H_2SO_4 0.5 mol L^{-1}. For comparative purposes, a commercial carbon supported Pt and PtRu catalysts from Etek® (20 wt.%; Pt:Ru molar ratio 1:1) was used.

3. Results and discussion

The results of the chemical titrations (Boehm method), collected in Table 1, show that the treatments with nitric acid produce changes in the chemical surface group content. This is probably because the very strong oxidizing character so that the activation energy to react with carbon is almost negligible [24]. The reaction with nitric acid introduces a very large amount of acidic groups. This is particularly relevant for carboxyls and phenols, although the amount of lactones is threefold larger than in the original sample.

The results of the BET surface area are summarized in Table 2. The BET surface area of the support decreased 44% after nitric acid treatment. It indicates that the treatment changed the carbon structure. A small reduction in the surface area of carbons after oxidants treatment was already observed [25]. The authors showed that the oxygenated groups are introduced in the carbon pore structure, resulting in a carbon pore blockage.

Table 1
Chemical surface groups (mequiv. g^{-1}).

Sample	Carboxyls	Lactones	Phenols	Basic
Vulcan XC72R	0.180	0.126	0.098	0.207
Vulcan XC72R-HNO_3	1.467	0.384	0.875	0.231

Table 2
Laser scattering particle size, BET and cyclic voltammetry surface area analysis obtained for the carbons support.

Carbon black	Laser scattering particle size (μm)	BET area ($m^2\,g^{-1}$)	Cyclic voltammetry area ($m^2\,g^{-1}$)
Vulcan XC72R	0.6	241	198
Vulcan XC72R-HNO_3	15	167	104

As previously showed [26–33] and demonstrated by the current FTIR results, oxidation treatments produce a large amount of oxygenated groups (carboxylic, hydroxyl, lactones, etc.) in the carbon surface. These groups are responsible for changing both the acid–basic character of the carbon black and the pore structure. The carbon black pore structure is of great importance in the development of support material for DMFC applications. Micropores filled with metal catalysts are undesirable as they restrict the access of the reactants to the active sites, resulting in waste of noble catalysts. It has been suggested that the oxygen surface groups fixed at the entrance of micropores after carbon functionalization, block the diffusion of species into the micropores. The same restricted diffusion effect in the carbon black micropores after a chemical treatment with hydrogen peroxide was already observed [34]. In this study, the blocking of the micropores can be seen from the BET results (Table 2).

XRD diffractograms of the studied carbon blacks displayed broad diffraction peaks occurring at $2\theta \approx 24^\circ$ and 43° that are related to (0 0 2) and (10×) peaks, respectively. The location and width of these two diffraction peaks indicate that the carbon black has a coke-like structure with disordered carbonaceous interlayers [35]. The occurrence of the same pore restriction in terms of XRD results can also be discussed [36]. The authors took into consideration the strain exerted by selected surface oxygen groups on the graphene layers. While filling the micropores and arranging themselves at an optimum distance to minimize the interatomic carbon repulsion. After the functionalization process, there was a change in the position of the peaks. This effect can be attributed to the incorporation of the oxygenated groups in the carbon black structure.

Fig. 1 displays the carbon particle size distribution obtained by the laser scattering technique. A reduction of the carbon black average particle size can be seen in Table 2. With the HNO_3 functionalization process, the carbon black became much more hydrophilic and consequently, the dispersion of the carbon black in water was easily achieved. The particle size of grafted carbon black

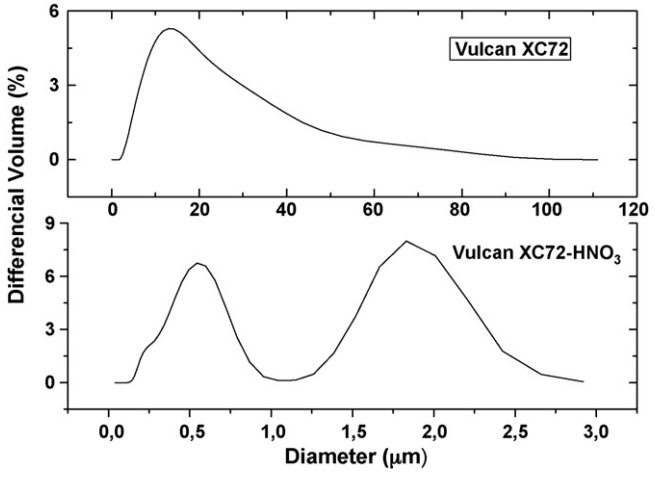

Fig. 1. Laser scattering particle size distribution for Vulcan XC72R and Vulcan XC72R-HNO_3.

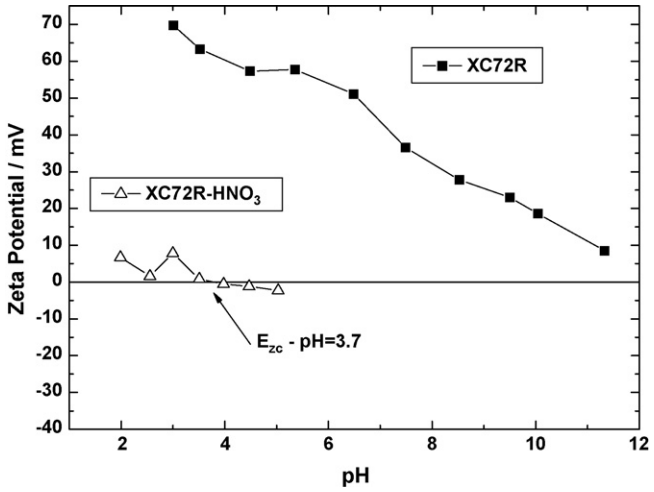

Fig. 2. Zeta potential vs. pH curves for the Vulcan XC72R as obtained and after functionalization.

dispersed in water is significantly smaller than the carbon black without grafting, thus indicating a beneficial behavior in terms of electrocatalyst preparation as well as for the final membrane–electrode-assembly preparation using electrocatalyst inks.

The thermo gravimetric analysis for the carbon black materials showed a gradual mass loss of about 4% on heating from 25 to 100 °C for the functionalized carbon black, which is attributed mainly to the loss of water. At the range of 100–1000 °C, there is a carbon black decomposition, probably associated with the adsorption of oxygenated species, like carbon monoxide, carbon dioxide and other volatile substances.

Fig. 2 shows the pH dependence of the zeta potential of the studied materials. A positive value of the zeta potential over the entire studied pH range was obtained for the carbon black without functionalization, without the presence of a isoelectric point or a E_{zc}. For the functionalized material, a reduction of the pH value for the E_{zc} was observed, 3.7 pH. An increase in the magnitude of the negative value of the zeta potential, attributed to the formation of acidic groups at the surface was also reported after oxidation of carbon fibers [37] and after oxygen plasma oxidation of mesocarbon microbeads [38].

Grundke et al. [37] observed the same behavior as found in the present study. They found an isoelectric point after oxidation of carbon fibers and attributed it to water adsorption competing with specific ion adsorption, which leads to a lower value for the maximum negative zeta potential.

Cyclic voltammograms at different sweep rates 5, 10, 20, 30, 40, 50, 60, 80, 100 mV s^{-1} (where in the graphic, the sweep rate for each curve is indicated by the arrows) obtained for the carbon black and C-HNO_3 are shown in Fig. 3. They illustrate the effects of the functionalization procedure and of the scan rate variation on the current–potential profiles. The date obtained from the plots of the anodic capacitive current I_c vs. ν (ν = sweep speed) (I_c values obtained at E = 0.8 V vs. RHE) were used for the calculation of the double layer capacitances and of the electrochemical active areas. These measurements were carried out at 0.8 V vs. RHE, because in this range the cyclic voltammetry current is essentially constant and related to double layer charging, since most surface redox active groups must be oxidized at lower potentials [39]. The currents were divided by the mass of the sample in order to allow easy comparison of the results.

It can be seen from Fig. 3 that the responses of the electrodes are those typically observed for several types of high surface area carbons [35,40]. For the C-HNO_3, the cyclic voltammetry currents

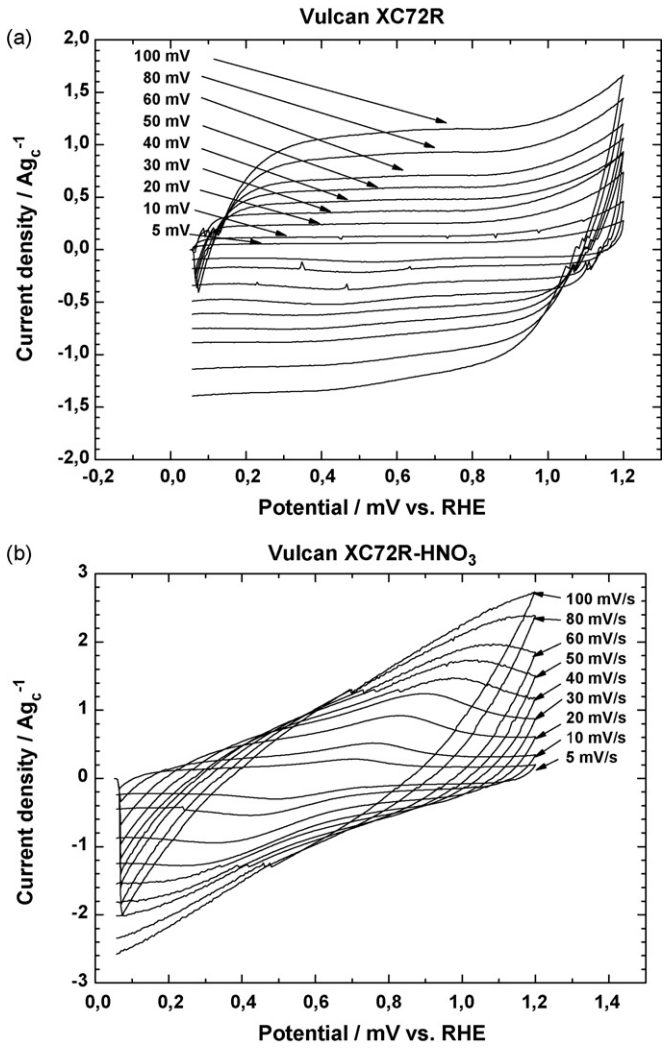

Fig. 3. Cyclic voltammograms at different sweep rates in H_2SO_4 0.5 mol L^{-1} for the Vulcan XC72R (a) as received and (b) after functionalization.

increase after the functionalization and this behavior is probably related to a breaking of hydrophobicity and/or to an increase in the amount of surface electrochemically active groups. From the voltammograms in Fig. 3b, it is observed that for the C-HNO_3 sample, the increase of scan rate leads to a distortion on the current–potential relationship, which is not observed for carbon black. This phenomenon is related to the presence of ohmic drop effects introduced by distributed resistance inside the electrode layer. This fact is confirmed by the plotted results of the I_c vs. ν, depicting the deviation of linearity at higher scan rates of some plots for the C-HNO_3.

The slope values obtained from the linear region (low scan rates) of the plots I_c vs. ν were used to estimate the electrochemically active surface area. These results are presented in Table 2, together with the corresponding values obtained from the BET measurements. The values of BET surface area obtained are similar to those obtained with cyclic voltammetry, which demonstrates the consistency of the results of the present study. The cyclic voltammetry surface area results are generally smaller than those obtained through BET. These results indicate that the surface changes introduced by the carbon functionalization lead to different effects in the adsorption process of N_2 in the BET and also of the electrolyte in the voltammetric analysis. Since the cyclic voltammetry area is strongly affected by the hydrophobic properties of the carbon surface, it is concluded that these results

Table 3
Pt:Ru atomic ratio (EDX analysis), particles size (from DRX and TEM), for the prepared electrocatalysts.

Electrocatalysts	Pt (wt.%)	Ru (wt.%)	Pt:Ru atomic ratio	Particle size (nm) DRX	Particle size (nm) TEM
PtRu/XC72R 20%	13.8	6.8	1:1	4.8	5.3
PtRu/XC72R-HNO_3 20%	13.8	6.8	1:1	3.2	3.8
PtRu/C E-TEK 20%	13.8	6.8	1:1	1.5	2.8

show that a small fraction of the total available carbon surface in the electrode layer is not electrochemically active.

The energy dispersive of X-ray (EDX) and the mean crystallite size results of the electrocatalysts are presented in Table 3. The Pt:Ru atomic ratios of the obtained electrocatalysts were very close to the nominal composition, calculated from the masses of the used metallic components.

The electrocatalysts showed diffraction peaks at about $2\theta = 40^\circ$, 47°, 67° and 82°, Fig. 4, characteristic of the *fcc* structure of platinum and platinum alloys carbon black Vulcan XC72 and its functionalized derivatives show the characteristic diffraction pattern of graphitic carbon ($2\theta = 25^\circ$), as discussed before. Moreover, neither peaks of separate tetragonal RuO_2 nor of hexagonal close-packed (*hcp*) Ru phases are found [41–44]. The average crystallite size, L, may be estimated according to the Scherer equation using the platinum peak (2 2 0) [22]:

$$L = \frac{0.9\lambda_{k\alpha 1}}{B_{(2\theta)} \cos\theta_{\max}} \quad (1)$$

where $\lambda_{k\alpha 1}$ is 1.54056 Å and $B_{(2\theta)}$ is in radians.

The XRD average crystallite size, when compared with the TEM average particle size, was very similar. The values of the average particle and crystallite size are presented in Table 3. These results show that the alcohol reduction produces nanoparticles in the desirable size range for fuel cell applications. Oxidation of the support did not lead to changes in the PtRu particle size. Agglomeration of small PtRu nanoparticles was found to occur on all materials. Hence, the slight discrepancy between particles size as determined from TEM and XRD techniques.

The TEM images are presented in Figs. 5–7 show a more homogenous and uniform particle distribution for the PtRu/C-HNO_3 material compared to the others. For the PtRu/C Vulcan XC72R material, the result was a product with a great deal of

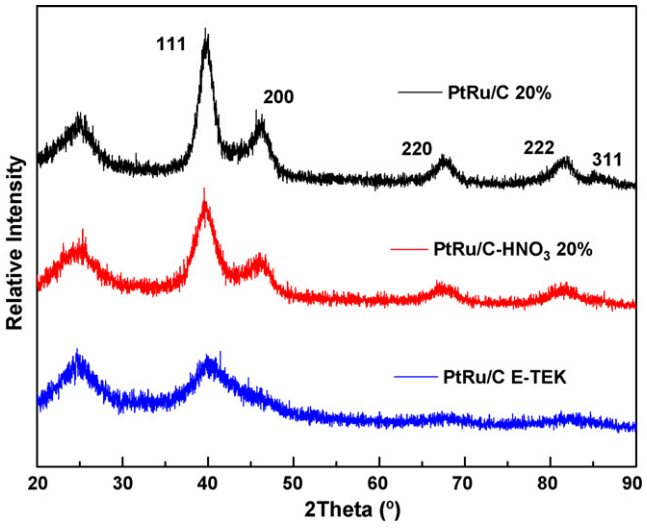

Fig. 4. X-ray diffractograms of the PtRu/C electrocatalysts.

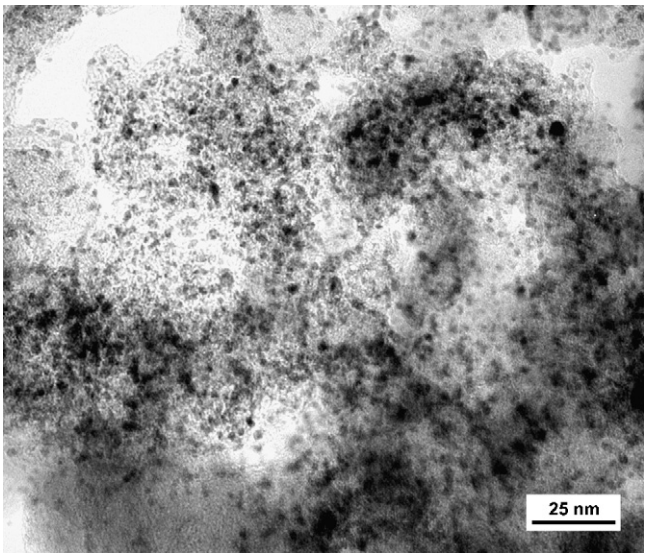

Fig. 5. Transmission electron microscopy micrograph for the PtRu/C Etek® material.

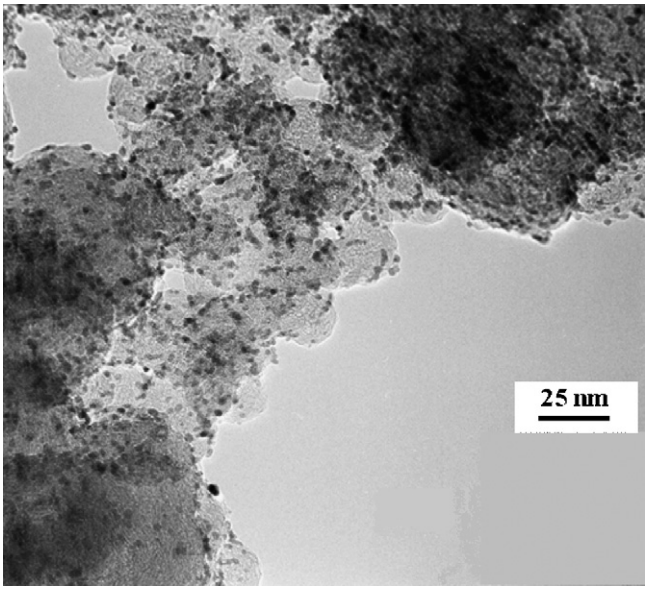

Fig. 6. Transmission electron microscopy micrograph for the PtRu/XC72R material.

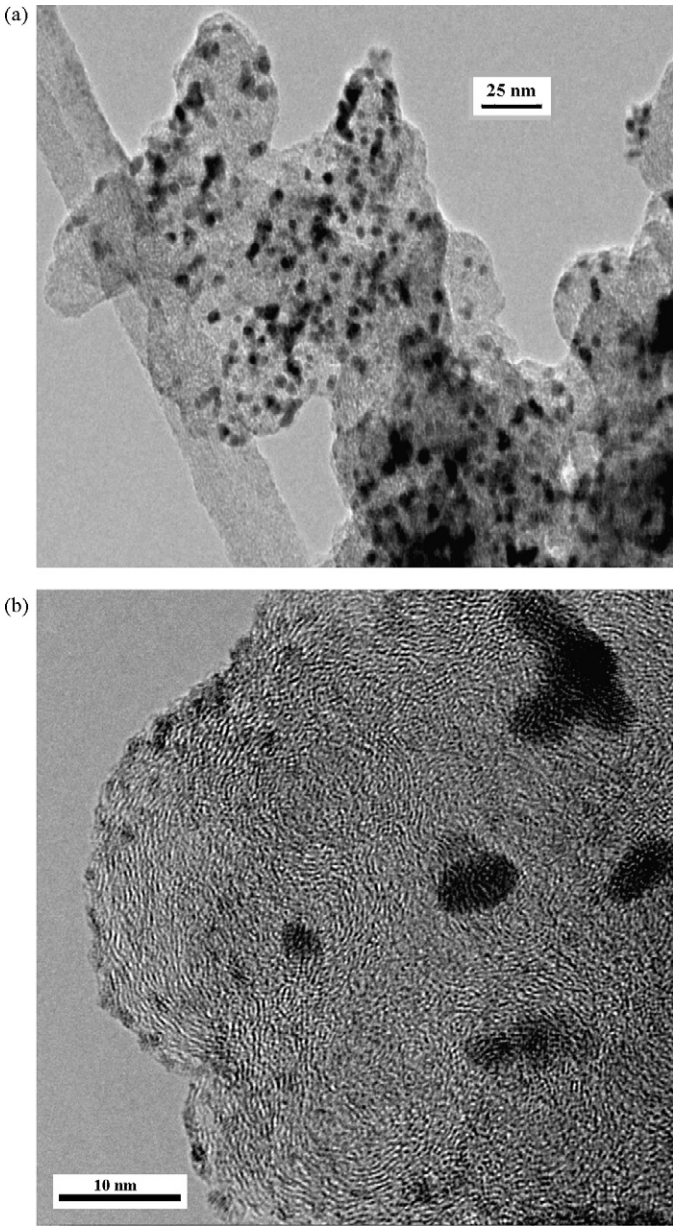

Fig. 7. (a) Transmission electron microscopy micrograph for the PtRu/XC72R-HNO_3 material and (b) high resolution transmission electron microscopy micrograph for the PtRu/XC72R-HNO_3 material.

agglomerates and no uniform particle distribution. The TEM particle size histograms are presented in Fig. 8 and the average particle size in Table 3. Compared to the commercial PtRu/C Etek® material, the electrocatalysts supported in functionalized carbon black present a more homogeneous distribution. In the commercial material, particles in the average range of about 2–3 nm correspond to no more than 40% of the particles, while for the functionalized carbon black material, in the average range (3–5 nm), the particles correspond to about 70%.

The cyclic voltammograms of PtRu/C 20% performed in 0.5 mol L^{-1} H_2SO_4 are shown in Fig. 9. The cyclic voltammograms show characteristics for typical PtRu/C catalysts [44]. It can be observed by these curves that for PtRu catalysts, the hydrogen UPD (underpotential desorption) region (0.075–0.35 V vs. RHE) is less defined, because the adsorption/desorption hydrogen peaks are not developed on Ru. Some differences are apparent between the materials, related to the different particle size between the catalysts and also related to the better catalyst nanoparticle utilization supported on the functionalized carbon black.

In Fig. 10 are presented the cyclic voltammetry (anodic sweep, first cycle) for 1 mol L^{-1} methanol oxidation in H_2SO_4 0.5 mol L^{-1}. It was discounted from each anodic sweep its respective base voltammograms (from Fig. 9), to avoid any misleading comparison or interference from the pure carbon support voltammogram.

This enhanced performance is explained by the better particle distribution in the PtRu/C-HNO_3 electrocatalyst and can also be inferred by the functional mechanism [45]. Due to the high affinity of Ru towards oxygen-containing species, sufficient amounts of OH_{ad} are formed to support reasonable carbon monoxide oxidation rates. This effect leads to higher activities for the overall methanol oxidation process on PtRu compared to Pt. This high activity on PtRu/C-HNO_3 can be better explained and understood by the oxygenated groups on the carbon surface. The enhanced performance can be also explained by the better

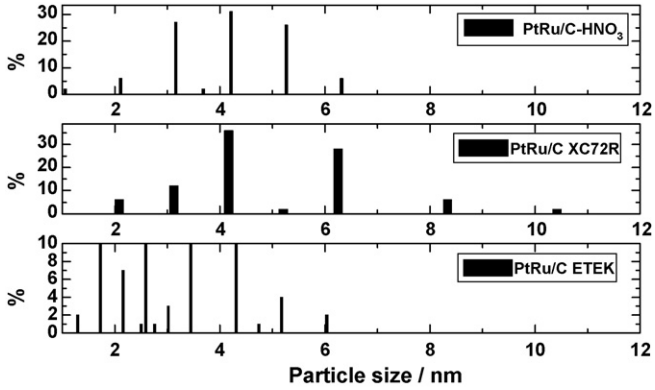

Fig. 8. Transmission electron microscopy particles size histograms for the electrocatalyst systems.

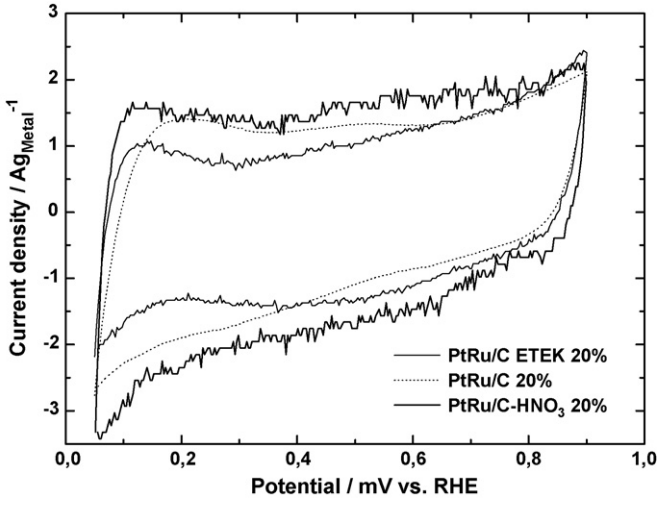

Fig. 9. Cyclic voltammograms in H_2SO_4 0.5 mol L^{-1}, 10 mV s^{-1} for the prepared electrocatalyst systems.

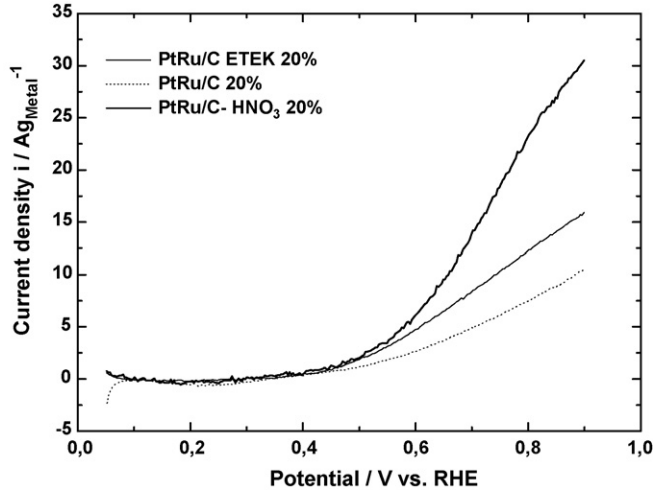

Fig. 10. Anodic stripping for methanol 1 mol L^{-1} oxidation in H_2SO_4 0.5 mol L^{-1} for the prepared electrocatalyst systems.

PtRu particle utilization. Considering that with the pore blockage effect, the nanoparticles are located outside the pore structure and now available for the oxidation reaction and diminishing the waste of noble catalysts.

4. Conclusions

BET results showed that the specific surface area for the carbon support after functionalization was reduced by 44%, which indicates that the treatment used produced significant changes in the carbon structure. It was suggested that the oxygen surface groups are fixed at the entrance of the micropores, after the carbon functionalization, blocking the diffusion of species into them. The XRD results showed that after the functionalization, there was a change in the location of the peaks. This effect can be attributed to the incorporation of the oxygenated groups in the carbon black structure. With the zeta potential results, using the functionalized material, a reduction of the pH value for the E_{zc} was observed. For the XC72R-HNO_3 sample the cyclic voltammetry currents increased after the functionalization. This behavior is probably related to a breaking of hydrophobicity and/or to an increase in the amount of surface electrochemically active groups. The TEM images reveal a very homogeneous and uniform particle distribution for the PtRu/C-HNO_3 material and a less homogeneous distribution for the PtRu/C Vulcan XC72R material. For the methanol oxidation results, an increase in the methanol oxidation current for the PtRu/C-HNO_3 electrocatalyst system was observed compared to the PtRu/C Etek® formulation. This can be explained due to the better nanoparticle distribution and better nanoparticle utilization in the Vulcan XC72R-HNO_3 functionalized support, enhancing the methanol oxidation reaction.

Acknowledgments

The authors wish to thank CAPES, DAAD, FINEP, IPT and IPEN, for financial and technical support.

References

[1] H. Wendt, M. Götz, M. Linardi, Química Nova 23 (4) (2000) 538–546.
[2] T. Frey, M. Linardi, Electrochim. Acta 50 (1) (2004) 99–105.
[3] M. Carmo, V.A. Paganin, J.M. Rosolen, E.R. Gonzalez, J. Power Sources 142 (1–2) (2005) 169–176.
[4] E.I. Santiago, V.A. Paganin, M. Carmo, E.A. Ticianelli, E.R. Gonzalez, J. Electroanal. Chem. 575 (1) (2005) 53–60.
[5] A. Oliveira Neto, E.G. Franco, E. Aricó, M. Linardi, Electrochim. Acta 22 (2004) 93–101.
[6] F. Colmati, E. Antolini, E.R. Gonzalez, Electrochim. Acta 50 (2005) 5496–5503.
[7] F.N. Buchi, W. Vielstich, A. Lamm, A.H. Gasteiger, Handbook of Fuel Cells, John Wiley and Sons, 2003.
[8] M. Watanabe, S. Motoo, J. Electroanal. Chem. 60 (1975) 275–283.
[9] F.J. Scott, C. Roth, D.E. Ramaker, J. Phys. Chem. C 111 (30) (2007) 11403–11413.
[10] M. Mastragotino, A. Mossiroli, F. Soavi, J. Electrochem. Soc. 151 (2004) 1919–1924.
[11] Z. Wang, G. Yin, P. Shi, Carbon 44 (2005) 133–140.
[12] F. Rodriguez-Reinoso, I. Rodriguez-Ramos, C. Moreno-Castilla, A. Guerrero-Ruiz, J.D. Lopez-Gongalez, J. Catal. 99 (1986) 171–183.
[13] F. Rodriguez-Reinoso, C. Moreno-Castilla, A. Guerrero-Ruiz, I. Rodriguez-Ramos, J.D. Lopez-Gongalez, Appl. Catal. 15 (1985) 293–300.
[14] S. Biniak, G. Szymanski, J. Siedlewski, A. Swiatkowski, Carbon 35 (1997) 1799–1810.
[15] B.K. Pradhan, N.K. Sandle, Carbon 37 (1999) 1323–1332.
[16] T. Zhicheng, L. Qiuye, L. Gongxuan, Carbon 45 (1) (2006) 41–46.
[17] H. Shioyama, K. Honjo, M. Kiuchi, Y. Yamada, A. Ueda, N. Kuriyama, T. Kobayashi, J. Power Sources 161 (2006) 836–838.
[18] M. Linardi, E.V. Spinacé, A. Oliveira-Neto, E.G. Franco, E.R. Gonzalez, Química Nova 27 (4) (2004) 648–654.
[19] M. Linardi, A. Oliveira-Neto, E.V. Spinacé, T.R.R. Vasconcelos, Br Patent PI 0304121-2 (2003).
[20] A.R. dos Santos, M. Carmo, A. Oliveira-Neto, E.V. Spinacé, J.G.R. Poco, C. Roth, H. Fuess, M. Linardi, Ionics 14 (2008) 43–51.
[21] H.P. Boehm, Carbon 32 (5) (1994) 759–769.
[22] P. Scherrer, Nach. Ges. Wiss 26 (1918) 98–109.
[23] E.V. Spinacé, A. Oliveira-Neto, T.R.R. Vasconcelos, M. Linardi, J. Power Sources 137 (2004) 17–23.
[24] J.M. Thomas, in: P.L. Walker, jr (Ed.), Chemistry and Physics of Carbon, Marcel Dekker, New York, 1965 (Chapter 3).
[25] P. Vinke, M. Van der Eijk, M. Verbree, A.F. Voskamp, H. Van Bekkum, Carbon 32 (1994) 675–686.
[26] J.P. Chen, S. Wu, Langmuir 20 (2004) 2233–2242.

[27] V. Gomez-Serrano, M. Acedo-Ramos, A.J. Jopez-Peinado, C. Valenzuela-Calahorrro, Thermochim. Acta 291 (1997) 109–115.
[28] B.R. Puri, in: P.L. Walker, Jr. (Ed.), Chemistry and Physics of Carbon, vol. 6, Marcel Dekker, New York, 1970, pp. 191–282.
[29] R.C. Bansal, J.B. Donnet, F. Stoeckli, Active Carbon, Marcel Dekker, New York, 1988, pp. 27–118.
[30] M.V. López-Ramón, F. Stoeckli, C. Moreno-Castilla, F. Marín, Carbon 37 (8) (1999) 1215–1221.
[31] J.A. Menéndez, J. Phillips, B. Xia, L.R. Radovic, Langmuir 12 (18) (1996) 4404–4410.
[32] G.G. Park, T.H. Yang, Y.G. Yoon, W.Y. Lee, C.S. Kim, Int. J. Hydrogen Energy 28 (2003) 645–650.
[33] P. Painter, M. Starcinic, M. Coleman, Fourier Transform Infrared Spectroscopy, vol. 4, Academic Press, New York, 1985, pp. 169–89.
[34] C. Moreno-Castilha, M.A. Ferro-Garcia, J.P. Joly, I. Bautista Toledo, F. Carrasco-Marin, J. Rivera-Utrilla, Langmuir 11 (1995) 4386–4392.
[35] K. Kinoshita, Carbon: Electrochemical and Physicochemical Properties, John Wiley and Sons, New York, 1988, pp. 86–166.
[36] B. Pradhan, N.K. Sandle, Carbon 37 (1999) 1322–1323.
[37] K. Grundke, M. Boerner, H. Jacobasch, Colloids Surf. 58 (1991) 47–56.
[38] K. Esumi, M. Sugiura, T. Mori, K. Meguro, H. Honda, Carbon 25 (1987) 821–828.
[39] S.A.M. Silva, J. Perez, R.M. Torresi, C.A. Luengo, E.A. Ticianelli, Electrochim. Acta 44 (1999) 3565–3574.
[40] J.P. Donnet, R.C. Bansal, M.J. Wang, Carbon Black: Science and Technology, Marcel Dekker, New York, 1993.
[41] C. Roth, N. Martz, H. Fuess, Phys. Chem. Chem. Phys. 3 (2001) 315–319.
[42] C. Roth, M. Goetz, H. Fuess, J. Appl. Electrochem. 7 (2001) 793–798.
[43] C. Roth, N. Martz, H. Fuess, J. Appl. Electrochem. 3 (2004) 345–348.
[44] M. Carmo, A.R. dos Santos, J.G.R. Poco, M. Linardi, J. Power Sources 173 (2007) 860–866.
[45] T.J. Schmidt, M. Noeske, H.A. Gasteiger, R.J. Behm, Langmuir 13 (10) (1997) 2591–2595.